Spatiotemporal dynamics of the spin transition in $[Fe(HB(tz)_3)_2]$ single crystals

Karl Ridier,[1] Sylvain Rat,[1] Helena J. Shepherd,[2] Lionel Salmon,[1] William Nicolazzi,[1] Gábor Molnár,[1,*] and Azzedine Bousseksou[1,†]

[1]*Laboratoire de Chimie de Coordination, CNRS UPR-8241, 205 route de Narbonne, F-31077 Toulouse, France*

[2]*School of Physical Sciences, University of Kent, Park Wood Road, Canterbury CT2 7NH, United Kingdom*

(Received 1 August 2017; published 11 October 2017)

The spatiotemporal dynamics of the spin transition have been thoroughly investigated in single crystals of the mononuclear spin-crossover (SCO) complex $[Fe(HB(tz)_3)_2]$ (tz = 1,2,4-triazol-1-yl) by optical microscopy. This compound exhibits an abrupt spin transition centered at 334 K with a narrow thermal hysteresis loop of ∼1 K (first-order transition). Most single crystals of this compound reveal exceptional resilience upon repeated switching (several hundred cycles), which allowed repeatable and quantitative measurements of the spatiotemporal dynamics of the nucleation and growth processes to be carried out. These experiments revealed remarkable properties of the thermally induced spin transition: high stability of the thermal hysteresis loop, unprecedented large velocities of the macroscopic low-spin/high-spin phase boundaries up to 500 μm/s, and no visible dependency on the temperature scan rate. We have also studied the dynamics of the low-spin → high-spin transition induced by a local photothermal excitation generated by a spatially localized (Ø = 2 μm) continuous laser beam. Interesting phenomena have been evidenced both in quasistatic and dynamic conditions (e.g., threshold effects and long incubation periods, thermal activation of the phase boundary propagation, stabilization of the crystal in a stationary biphasic state, and thermal cutoff frequency). These measurements demonstrated the importance of thermal effects in the transition dynamics, and they enabled an accurate determination of the thermal properties of the SCO compound in the framework of a simple theoretical model.

DOI: 10.1103/PhysRevB.96.134106

I. INTRODUCTION

Spin-crossover (SCO) solids are archetypal examples of multifunctional molecular materials that exhibit bistability between the so-called high-spin (HS) and low-spin (LS) electronic configurations [1,2]. The SCO phenomenon can be triggered reversibly by a variety of external perturbations (temperature change, application of pressure, intense magnetic field, light irradiation, etc.), and it involves spectacular changes in the physical properties (optical, magnetic, mechanical, and electrical). The molecular spin state change in bulk solids gives rise to elastic interactions between the labile molecular units, leading to the emergence of cooperative effects such as first-order phase transitions, associated hysteresis phenomena, and heterogeneous phase separation. The understanding and the control of the dynamics of first-order phase transitions is a general and appealing problem from a fundamental point of view and for technological applications as well [3]. The spatiotemporal characteristics of these phase transitions are indeed essential to interpret the ensuing phenomena as they are directly related to the mechanistic details of the switching of their physical properties. In the case of strongly cooperative SCO systems, singular phenomena and dynamics come into play during the transition within the thermal hysteresis region, including nucleation and growth processes [4–7], reversible photocontrol of the LS/HS phase boundary motion [8–10], (bidirectional) photoswitching induced by pulsed laser excitations [11–13], and subsequent "cascade" phenomena [14]. In all these processes, the nonequilibrium structural domain evolution turns out to be one of the key aspects of these phase transitions.

In the past decade, many studies have been devoted to the microscopic observation of the *spatiotemporal aspects* of the spin transition in cooperative SCO single crystals, either by optical microscopy [6–10,14–27] or Raman microspectroscopy [6,28]. These investigations revealed a universal phase separation mechanism with the formation of predetermined heterogeneous nuclei (induced by light irradiation or temperature change) and the existence of moving macroscopic domain walls with low propagation velocities (typically $\sim 1-20\,\mu m\,s^{-1}$ [7,8,14,20,22]). They also put into evidence the important role of crystal defects, strain, and microstructure in the spatiotemporal development of the spin transition, making this process deeply crystal-dependent [21,23]. In spite of their usefulness, these analyses are scarce and often difficult to interpret because of a lack of *quantitative* and *reproducible* experimental observations. This issue mainly arises from the limited number of robust, high-quality single crystals (showing a strong resilience upon repeated switching), which represents a major obstacle for a deeper investigation of the spatiotemporal dynamics of the spin transition in such SCO solids. From a theoretical point of view, the understanding of the phase transition dynamics is also hindered by the low predictive power of current models, which often use many experimentally inaccessible parameters.

In this article, we report on an optical microscopy investigation of the spin-transition dynamics in single crystals of the mononuclear complex $[Fe(HB(tz)_3)_2]$ (tz = 1,2,4-triazol-1-yl) (1). Single crystals of this compound, which were recently obtained in their solvent-free form [29], are known to exhibit an extremely abrupt first-order spin transition centered around 334 K associated with a narrow (∼1−K-wide) thermal hysteresis loop. Such crystals have the particularity of showing unprecedented resilience upon repeated switching, which enabled a series of experiments based on individual

*gabor.molnar@lcc-toulouse.fr,

†azzedine.bousseksou@lcc-toulouse.fr

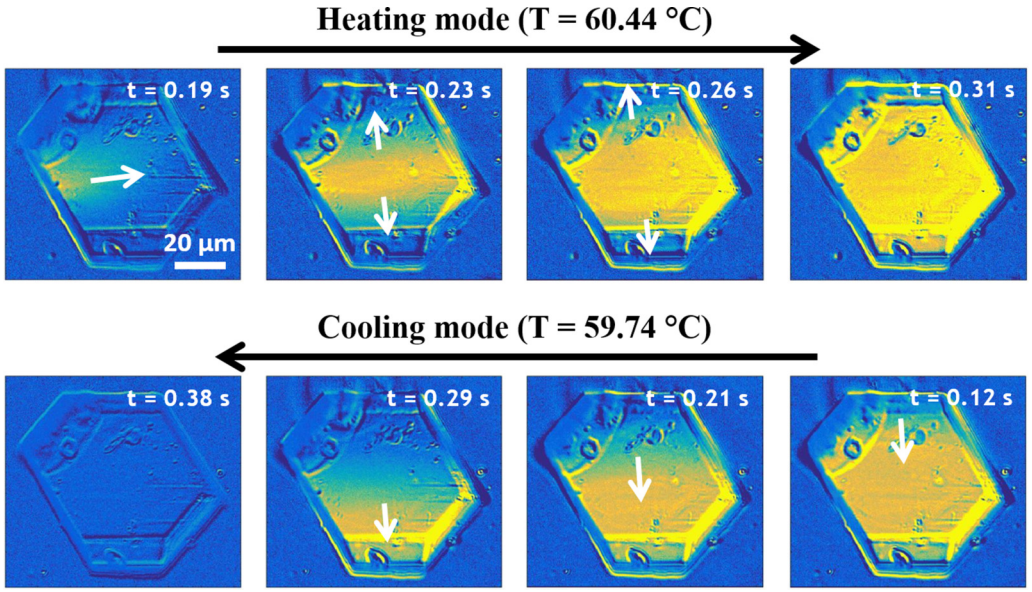

FIG. 1. Selected optical microscopy snapshots (in bright-field transmission mode at 543 ± 22 nm) of the thermally induced spin transition of crystal *A* in the heating and cooling modes (0.5 °C/min). The LS → HS and HS → LS transitions occur at 60.44 and 59.74 °C, respectively, the transition process being considered isothermal due to the large velocity of the front interfaces (see the text). Arrows indicate the propagation directions of the phase boundaries. To better display the phase-separation phenomenon, images are processed by subtracting the low-temperature image of the crystal (in the pure LS state) from each of them. Blue and dark yellow (artificial) indicate the LS and HS phase, respectively. The movies (S1a and S1b) are available in the Supplemental Material [31].

single crystals to be carried out. Herein, we have investigated the spatiotemporal dynamics of the spin transition induced by a temperature change, and a local photothermal excitation generated by a localized (Ø = 2 μm) laser beam. The present analyses reveal unusual and singular features compared to those reported in the literature.

II. EXPERIMENTAL METHODS

A. Crystal synthesis

Single crystals of (1) were synthesized as described previously by Rat *et al.* [29]. This compound crystallizes in the orthorhombic *Pbca* space group, and all crystals have a characteristic hexagonal shape as shown in Fig. 1. X-ray-diffraction analyses identify the *c* axis as being normal to the large planar face. Crystallographic data show that the LS and HS phases are isostructural, but a remarkably strong anisotropic deformation of the unit cell is evidenced during the spin transition, with the volume change occurring mainly along the *c* axis.

B. Optical microscopy measurements

The crystals were enclosed in a variable-temperature THMS600 microscope stage (Linkam Scientific Instruments), which was purged with dry nitrogen for at least 15 min prior to the measurements. Hereafter, the temperature of the microscope stage (and the surrounding nitrogen atmosphere) monitored by the controller will be denoted as the "bath" temperature T_b. Optical microscopy images of crystals were recorded in bright-field transmission mode using an Olympus BX51 microscope equipped with a × 50 magnification objective (numerical aperture, NA = 0.5) and either a high-speed Zyla 5.5 megapixel sCMOS camera (Andor Technology, 2560 × 2160 pixels of 6.50 µm size) or a Clara CCD camera (Andor Technology, 1392 × 1040 pixels of 6.45 µm size). The sample was illuminated by a halogen lamp (400–700 nm), but the spectral range was reduced using a band-pass filter (543 ± 22 nm) where the optical density contrast is maximum between the LS and HS states. Images and videos were treated using IMAGEJ software [30].

Spin transitions were also triggered by a laser beam (through photoheating process) using a He-Ne (λ = 632.8 nm) continuous laser (Melles Griot) coupled to the optical microscope. Using the ×50 long working distance microscope objective, the laser beam was focused on the crystal to a spot with a diameter of ∼2 μm. The sample was mounted on a motorized stage with a resolution of 0.1 µm, allowing accurate control of the position of the irradiated area on the crystal. The laser light was filtered out using a notch filter (centered at λ = 633 nm) installed in front of the camera. Nevertheless, a small residual laser intensity was always detected during the experiments.

III. RESULTS AND DISCUSSION

A. Spatiotemporal aspects of the thermally induced spin transition

In this first part, we investigated in detail the spatiotemporal dynamics of the thermally induced spin transition of (1). Optical microscopy images of the same crystal, denoted *A* (∼90 × 60 × 35 μm^3 size), have been recorded (with a high frame rate of 285 Hz) during successive heating-cooling cycles at different temperature scan rates ranging from 0.1 to 5 °C/min. This optical microscopy study clearly demonstrates the phase separation phenomenon associated with a

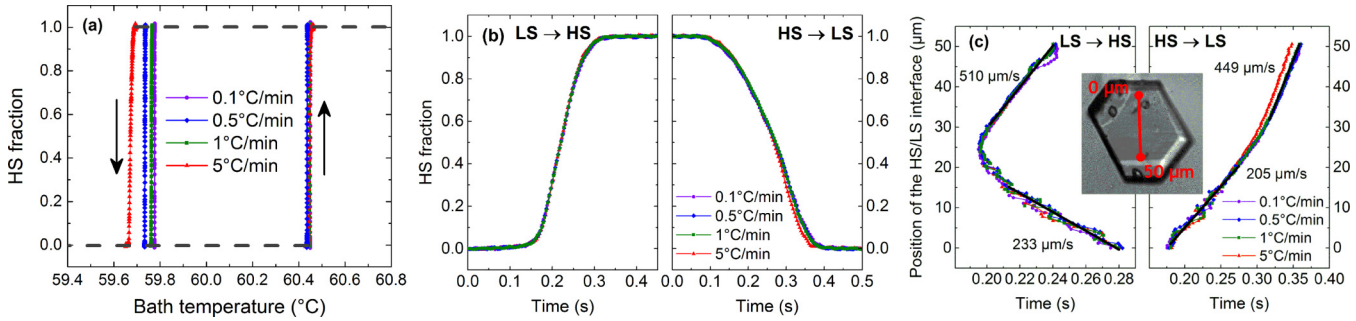

FIG. 2. Spatiotemporal characteristics of the thermoinduced spin transition in crystal A of (1) recorded at various temperature scan rates. The HS fraction is determined from the spatially averaged optical transmission of the entire crystal measured by optical microscopy with a high frame rate (fps = 285 Hz). (a) Thermal evolution of the HS fraction of crystal A over successive heating-cooling cycles. (b) Evolution of the HS fraction as a function of time during the LS → HS (heating mode) and HS → LS transition (cooling mode). (c) Evolution of the mean position of the LS/HS phase boundary along the red line (shown in the inset) as a function of time during heating (LS → HS) and cooling (HS → LS) modes. The corresponding phase-boundary velocities are indicated in the figure.

heterogeneous nucleation process and the ensuing formation of a moving phase boundary. As shown in Fig. 1, the nucleation of the LS and HS phases occurs at different places in the solid. In the heating mode, the nucleus of the HS phase is located at the left edge (in the middle of the crystal) and two phase boundaries are observed, propagating toward the two ends of the crystal. In the cooling mode, the nucleation of the LS phase occurs at the top edge of the crystal, and the phase boundary propagates across the entire sample. These features were observed in a very reproducible manner for each thermal cycle.

Microscopy images show that the LS/HS phase boundaries do not form narrow well-defined straight lines, as has often been reported in other SCO compounds [14,22,26]. Instead, the interfaces appear to be broad and quite diffuse. Nevertheless, this feature may be exacerbated due to their high propagation velocities (*vide infra*), and, in the case of crystal A, the large thickness of the sample (∼35 μm), which might imply a tilted domain wall in the studied (a,b) plane. As displayed in Fig. 1, the macroscopic interfaces seem, however, to have a unique and reproducible orientation, during both the LS → HS and HS → LS transitions. As discussed by Sy *et al.* [22], this could be an intrinsic feature of the system that tries to minimize its excess elastic energy caused by the lattice mismatch between the coexisting phases during the transformation. Such considerations may also explain the anisotropic domain growth observed during the LS → HS transition in crystal A, where the newly formed HS phase propagates first in the "horizontal" direction because it is energetically favorable for the system to form the domain wall in that particular orientation, the growth then occurring in the perpendicular direction. We did not succeed in correlating the reproducible orientation of the phase boundary with the structural data and the expected "mismatch-free" direction in the (a,b) plane. As a matter of fact, crystal A is certainly not favorable for this kind of study because of its relatively small size, which makes the face indexing arduous. In spite of that, remarkable quantitative measurements can be made on the transition kinetics of the crystal. These results are presented in Fig. 2.

Figure 2(a) shows the evolution of the normalized spatially averaged optical transmission of the crystal, which can be related to the HS fraction, as a function of the bath temperature (displayed by the controller) during successive thermal cycles recorded at various scan rates. These measurements show the existence of stable rectangular hysteresis loops (∼0.8 K wide) with extremely abrupt transitions. The thermal hysteresis loops are obtained with high reproducibility, and the transition temperatures ($T_{1/2}{}^{\uparrow} = 60.45 \pm 0.01\,^{\circ}$C and $T_{1/2}{}^{\downarrow} = 59.70 \pm 0.05\,^{\circ}$C) have a very low dependency on the temperature scan rate. The most striking result is presented in Fig. 2(b), where the HS fraction is plotted as a function of time. It shows that the transition kinetics of the crystal (in both the LS → HS and HS → LS directions) are strictly independent of the temperature scan rate in the studied range $0.1 - 5\,^{\circ}$C/min (factor 50), although a slight deviation is observed in the HS → LS transition curve at $5\,^{\circ}$C/min. Whatever the temperature scan rate, the transformations were completed within short periods of time: $\Delta t_{\mathrm{LS}\rightarrow\mathrm{HS}} \sim 0.15$ s and $\Delta t_{\mathrm{HS}\rightarrow\mathrm{LS}} \sim 0.25$ s, signaling fast switching processes.

Figure 2(c) displays the mean position of the phase boundary along a line crossing the crystal (see the inset) as a function of time in both the LS → HS and HS → LS directions. For each point of the crossing line, the procedure consists in identifying the time for which the HS fraction is $n_{\mathrm{HS}} = 0.5$. In accordance with the results presented in Fig. 2(b), the obtained position versus time curves do not show any temperature scan rate dependency. These curves reveal large velocities for the HS/LS phase boundary up to 510 μm s^{-1}, confirming the remarkable abruptness of the spin transitions of (1). Note that in the first stage of the LS → HS transition in crystal A, velocities as large as 850 μm/s have been even extracted in the horizontal direction. Interestingly, we can also notice that, in both LS → HS and HS → LS transformations, a significant difference is observed in the velocity of the phase boundary in the "upper" (0−25 μm) part and "lower" (25−50 μm) part of crystal A. This difference is not caused by thermal inhomogeneities because it was observed both on heating and cooling modes as well as when turning the crystal upside down on the heating stage. It should rather be attributed to the existence of structural defects within the solid, which are discernible in the optical microscopy images. Overall, such large velocities (typically 200−500 μm s^{-1}) have been evidenced, without any exception, in all crystals of compound (1) (as an example, see the data recorded on another crystal, denoted B, in Sec. 1 of the Supplemental Material [31]).

These observations refute the general belief that the propagation of domains is intrinsically slow in SCO solids ($1-20\,\mu m\,s^{-1}$) [7,8,14,19] compared to other compounds exhibiting first-order structural phase transitions, as in perovskite materials [32] or first-order metal-insulator transitions such as in VO_2 [33]. In these latter compounds, velocities larger than $1\,mm\,s^{-1}$ have been recorded. Recently, initial indications for the possibility of large transformation velocities in some SCO crystals have been reported [26,34], but, in the present study, such large velocities are measured in a systematic and reproducible manner with clear independence of the heating/cooling scan rate.

The present results should be compared with those obtained recently by Traiche *et al.* [27], who studied the kinetic aspects of the thermally induced spin transition in single crystals of [{Fe(NCSe)(py)$_2$}$_2$(m-bpypz)]. The authors demonstrated a clear widening of the thermal hysteresis loop and a sizable change in the propagation velocities of the LS/HS interface with the temperature scan rate. These results are in total contradiction with our observations. This strong difference might be due to the fact that our experiments were not carried out in vacuum but in a pure nitrogen atmosphere, which allows a better thermalization of the sample with the cryostat bath (this point will be discussed in the next part of the article). However, the problem of thermalization is certainly not the only factor because other compounds studied under the same experimental conditions (nitrogen atmosphere) exhibit clear scan-rate-dependent transition kinetics. This observation is shown in Fig. SI-4 (Sec. 2 of the Supplemental Material [31]), where we have carried out comparative optical microscopy measurements on single crystals of the compounds [Fe(bbpya)(NCS)$_2$] and [Fe(bapbpy)(NCS)$_2$]. This demonstrates that the scan rate independence is an intrinsic characteristic of the transition dynamics of (1), and that, contrary to the other studied compounds, (1) presents an example of the most interesting scan-rate-independent regime in which we deal with the genuine quasistatic thermal hysteresis loop.

The different spatiotemporal characteristics of the thermoinduced spin transition described herein for crystal *A* (e.g., stability of the thermal hysteresis loop, large velocities of the LS/HS phase boundaries, and no visible temperature scan rate dependency) were observed reproducibly upon 100 thermal cycles and with the same repeatability in most studied single crystals of (1). (For instance, see the complete study of the spatiotemporal dynamics carried out on a second crystal denoted *B* in the Supplemental Material [31].) Furthermore, crystals of (1) do not exhibit any apparent deterioration or irreversible effects (cracks, fractures, dislocations) in optical microscopy, signaling their exceptional resilience upon repeated switching. This is a rare feature since SCO crystals are often brittle and show visible damage after only a few thermal cycles [18,20]. The origin of the strong robustness of the crystals of (1) appears to be a key point to explain their singular spatiotemporal characteristics evidenced during the spin transition, since these two properties are undoubtedly correlated.

It is a difficult task to unambiguously determine the intrinsic properties at the origin of the strong resilience and the singular transition dynamics of the crystals of (1). In fact, many properties (e.g., mechanical, thermal, structural, and morphological) might have an impact on the observed features. Mechanical (elastic) properties have to be considered because large elastic modulus (stiffness) is known to be an essential ingredient for cooperativity [35]. Information about the lattice stiffness of (1) could be extracted through measurement of the Debye temperature ($\theta_D = 198$ K in the LS state [29]) from Mössbauer data [36]. This value is quite large compared to those obtained in many molecular SCO compounds [37], but it certainly cannot explain the uniqueness of the observed phenomena. The study of thermal properties is also of great importance because a large thermal conductivity implies low temperature gradients in solids and thus works in favor of fast transitions and strong robustness of materials. The influence of thermal properties will be investigated in more detail in Sec. III B, but their real impact on the thermally induced nucleation and growth mechanism remains poorly understood. Another extrinsic parameter to consider is the morphology of the studied samples. Large crystals favor the appearance of defects, whose effect is unfavorable to the propagation of dislocations, resulting in brittle solids. Conversely, small crystals, such as those studied here ($V \sim 1 \times 10^5\,\mu m^3$), are generally of better quality and allow for better thermalization and a more efficient thermal coupling with the external environment.

With regard to the structural properties, this SCO complex is somewhat unusual in that it is neutral, sublimable [38], and the crystals are free from solvent molecules or counterions that allow the formation of numerous short intermolecular contacts between adjacent SCO molecules [29]. The proven robustness of the crystals of (1) is presumably related to the dense packing and the existence of a tridimensional network of intermolecular contacts, which generate both long- and short-range elastic interactions between the SCO molecules and act in favor of the strong abruptness of the phase transition. Moreover, it is worth mentioning that the LS and HS phases are isostructural, which is probably favorable for rapid and abrupt spin transitions. An important feature often presumed as being responsible for the brittleness of SCO crystals and the slow transformation process is related to the relatively large change in unit-cell volume experienced by crystals during the spin transition. In (1), the spin transition is accompanied by a relative volume change of ~4.5% [29]. This value falls within the typical range of ferrous SCO materials (2–10 %) and thus it cannot explain its remarkable properties. However, more importantly, a crucial characteristic that reinforces the resilience of SCO crystals is the *anisotropic* character of the structural deformation and the emergence of possible mismatch-free directions during the phase transformation. Indeed, a strong anisotropic deformation allows the crystal to better accommodate the volume change (thus minimizing the elastic energy) throughout the phase transition. The changes of the unit cell along the crystallographic axes in (1) during the LS $\rightarrow$ HS transition are anisotropic and of opposite sign, with $\Delta a/a = -2.3\%$, $\Delta b/b = 1.0\%$, and $\Delta c/c = 5.6\%$ [29]. The result is that the volume increase originates mainly from expansion along the *c* axis, which is the direction of view in optical microscopy images displayed in Figs. 1 and 3. The fact that the relative expansions along the three axes are not of the same sign allows the crystal to channel a part of the internal frictions inherent to the LS/HS interface propagation. It is interesting to note that the compound [{Fe(NCSe)(py)$_2$}$_2$(m-bpypz)] shows an anisotropic structural deformation and a strong resilience upon switching as well

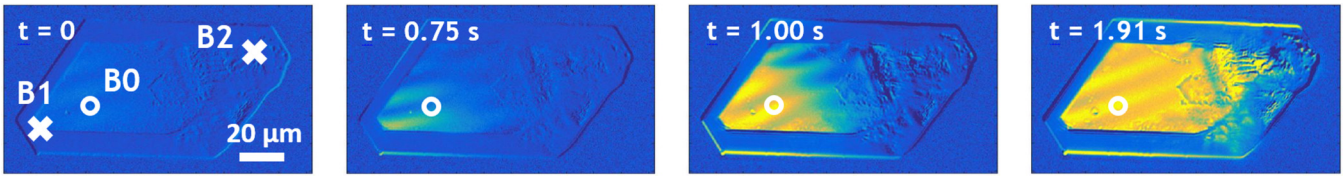

FIG. 3. Selected optical microscopy snapshots (recorded in bright-field transmission mode at 543 ± 22 nm) of the LS → HS transition of crystal B induced by a laser beam ($P = 205\,\mu$W) at $T_b = 60.6\,^{\circ}$C. The white circles indicate the area irradiated by the laser beam (point $B0$). The laser was turned on at $t = 0$ but the transition started at $t = 0.75$ s in the present conditions. Points $B1$ and $B2$ indicate the nucleation site of the HS state during the laser-induced process and the thermally induced transition, respectively. To better display the phase-separation phenomenon, images are processed by subtracting the initial image of the crystal in the complete LS state from each of them. Blue and dark yellow (artificial) indicate the LS and HS phase, respectively. The movie (S3) is available in the Supplemental Material [31].

[8,22]. Finally, an important ingredient for rapid transition dynamics is the absolute temperature of the transition. The high transition temperature of crystals of (1) increases the molecular switching rate and certainly favors the rapid motion of the LS/HS phase boundary.

One of the most singular features in the spatiotemporal development of the thermally induced spin transition of (1) is that the transformation kinetics of the crystal does not depend on the heating/cooling scan rate. This may indicate that the front propagation mechanism would not be related to a thermally activated process, but rather to a purely "cascade" phenomenon driven by strong elastic interactions between the SCO molecules. However, it should be stressed that the temperature variation ΔT that the crystal undergoes during its transformation is very small. For example, considering the fastest heating/cooling scan rate ($R = 5\,^{\circ}$C/min), we estimate that the crystal temperature has varied by about $\Delta T = R \times \Delta t = 12$ and 21 mK during the LS → HS and HS → LS transitions, respectively. This is in accordance with the abruptness of the thermal hysteresis cycles shown in Fig. 2(a). It means that, whatever the scan rate (from 0.1 to 5 °C/min), the thermally induced spin transition in the crystals of (1) can be safely described as an *isothermal* process. In other words, we are not able to address the effects of an apparent thermal activation process in the present experimental conditions. To further analyze the influence of thermal (activation) processes in the nucleation and growth phenomenon of (1), we have extended these spatiotemporal studies to spin transitions induced by a localized laser beam through a photoheating process.

B. Photo-thermo-induced transition generated by a spatially localized laser beam

In this second part, we have used a subtle approach that consists of generating the phase transition by a spatially localized photothermal excitation induced by a continuous He-Ne laser beam ($\lambda = 632.8$ nm, spot diameter $\sim 2\,\mu$m). This approach, introduced only recently [9,14,24], enables the deposition of a small and controlled amount of energy (heat) at a precise place of the crystal, and it allows us to investigate its spatiotemporal response in fine detail. A series of optical microscopy experiments have been conducted on a second crystal of (1), denoted B, by varying the bath temperature T_b and the laser power P. The spatiotemporal characteristics of the thermally induced spin transition of crystal B are presented in the Supplemental Material [31]. It reveals very similar features (e.g., strong resilience, a stable thermal hysteresis loop, large velocities of the macroscopic LS/HS interfaces, and no visible temperature scan rate dependency) to those of crystal A presented in Sec. III A. It should be stressed that the thermal hysteresis loop of crystal B is shifted slightly toward higher temperatures (∼0.8 °C) compared to crystal A due to a modified experimental setup, which lowers the light intensity of the microscope received on the sample.

1. *In quasistatic conditions*

We have performed a series of optical microscopy measurements at $T_b = 60.6\,^{\circ}$C (inside the thermal hysteresis loop) to investigate the spatiotemporal dynamics of the LS → HS transition at various powers of the laser beam localized at a given point (denoted $B0$) of crystal B. Before each measurement, the crystal was initially prepared in the LS state (great care was taken to wait at least 5 min in order to be at thermal equilibrium), and the laser was turned on at $t = 0$. The spatiotemporal evolution of the optical transmission was followed by optical microscopy. Figure 3 displays selected transmitted light microscopy images of the crystal during the laser-induced LS → HS transition with a power $P = 205\,\mu$W. Interestingly, we observe that the laser-induced nucleation site of the HS phase (point $B1$) does not coincide with the natural nucleation site (point $B2$) evidenced from the thermally induced studies (see the Supplemental Material [31]), and it is not located at the position of the laser spot either. It occurs instead at the bottom left corner of the crystal (point $B1$ located at $r_1 \approx 30\,\mu$m from $B0$), and the LS/HS phase boundary propagates across the entire crystal to reach the other end. It is interesting to note that the nucleation of the HS state does not occur at the laser spot, although the crystal temperature is the highest at that place. This observation is attributed to the existence of local elastic stresses, which prevent the nucleation process in the middle of the sample, while the edge of the crystal is a more favorable place where the accommodation strain with the parent phase is reduced [14].

The kinetics of the laser-induced spin transitions have been followed as a function of the laser power. The results are presented in Fig. 4(a), where the normalized spatially averaged optical transmission of the crystal (related to the HS fraction) is plotted as a function of time for various laser powers. The first observation is that the crystal is completely transformed in the HS state under the action of the spatially localized laser beam. However, at a given bath temperature, we note the existence

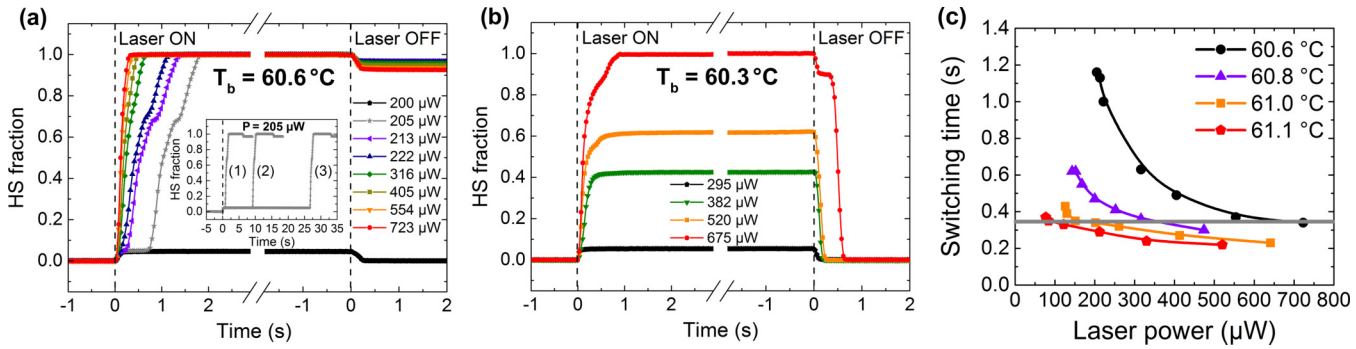

FIG. 4. Kinetics of LS → HS transitions of crystal *B* induced by a localized laser beam at two different bath temperatures: (a) $T_b = 60.6\,^{\circ}$C (inside the thermal hysteresis loop) and (b) $T_b = 60.3\,^{\circ}$C (out of the thermal hysteresis loop). Evolution of the normalized optical transmission (equivalent to the HS fraction) as a function of time at various laser powers. The small steps observed when turning on (off) the laser are due to a residual laser light intensity caught by the camera. Inset of (a): series of three measurements (chronologically denoted 1 to 3) performed under identical irradiation conditions ($T_b = 60.6\,^{\circ}$C and $P = 205\,\mu$W, threshold power). (c) Evolution of the switching time of crystal *B* as a function of the laser power at different bath temperatures. Lines are guides for the eye. The horizontal gray line indicates the LS → HS transition time of crystal *B* during the thermally induced process.

of a threshold power below which no LS → HS conversion is observed. At $T_b = 60.6\,^{\circ}$C, the threshold power is $\sim 205\,\mu$W. For higher powers, the complete conversion of the crystal is evidenced.

As shown in Fig. 4(a), a second important finding is that the transition kinetics at 60.6 °C depend strongly on the laser power. Near the threshold power ($P = 205\,\mu$W), the LS → HS transition of the crystal is complete within $\Delta t \approx 1.16$ s—with visible slow-down and acceleration stages in the transition curve—and occurs after a noticeable incubation period of ∼0.75 s (see also Fig. 3). When increasing the laser power, the incubation period becomes unmeasurable (below the temporal resolution of the camera) and the transition becomes much more abrupt ($\Delta t \approx 0.34$ s at $P = 723\,\mu$W, i.e., comparable switching kinetics to the thermoinduced process). Contrary to what was suggested by the thermally induced experiments in Sec. III A, these investigations demonstrate that the propagation of the HS/LS phase boundary depends on the laser power and is thus a genuine thermally activated process. Quantitatively, the mean velocity of the interface is found to be $\sim 99\,\mu\mathrm{m\,s^{-1}}$ at $P = 205\,\mu$W (threshold power) and increases up to $\sim 338\,\mu\mathrm{m\,s^{-1}}$ at $723\,\mu$W (note that the average velocity was found to be $\sim 320\,\mu\mathrm{m\,s^{-1}}$ during the thermally induced process; see the Supplemental Material [31]). The relatively low velocities observed at low laser power at $T_b = 60.6\,^{\circ}$C reveal that the driving force (arising from the difference in the free energies of the two phases) for the LS/HS phase boundary propagation is small, certainly because the crystal temperature is close to the Maxwell point T_{eq} (corresponding to the equilibrium temperature of the first-order transition for which the free energies of the two phases are equal [8]). As shown in Fig. 4(a), a trapping barrier for the front propagation is clear at a given HS fraction of the crystal ($n_{HS} \approx 0.68$), which is not visible for higher powers or during the thermoinduced transformation due to a larger driving force.

Another striking observation is the existence of a particular regime—close to the threshold laser power—for which long incubation periods (of the order of one second to several tens of seconds) are observed. The inset of Fig. 4(a) shows that for the same irradiation conditions ($T_b = 60.6\,^{\circ}$C and $P = P_{th} = 205\,\mu$W), the incubation period varies greatly from one measurement to another, increasing up to ∼30 s. In each case, after the incubation period, the transition kinetics are identical, confirming similar irradiation (thermal) conditions. Such long and different incubation periods cannot be related to the thermalization process of the crystal. Instead, this observation shows that the sample is in an extremely critical regime in which nucleation of the HS phase can be randomly triggered by small fluctuations (either intrinsic or due to the experimental conditions: laser, thermal fluctuations of the variable-temperature stage, etc.), confirming the stochastic nature of the heterogeneous nucleation process. Indeed, microscopic fluctuations of the HS phase may happen (through photoheating processes) and decay continuously until an unusually large fluctuation makes the HS phase grow over a critical nucleus size—stabilized by interactions between the newly formed HS species—making it more favorable to expand than to shrink back. The system then becomes strongly unstable, and the transformation process switches from stochastic to cooperatively deterministic, as predicted by theoretical models [39] and confirmed by the similar switching kinetics displayed in the inset of Fig. 4(a).

To further analyze the effect of the thermal activation process in the LS → HS transformation of crystal *B*, we repeated the measurements presented in Fig. 4(a) at three other bath temperatures (60.8, 61, and 61.1 °C) within the thermal hysteresis loop. For each of these bath temperatures, the existence of a threshold power and long incubation periods have been evidenced. Figure 4(c) summarizes the evolution of the transformation time of the crystal as a function of the laser power for each temperature. When the bath temperature T_b is close to $T_{1/2}^{\uparrow} = 61.26\,^{\circ}$C, the transition is fast regardless of the laser power, and it becomes even faster than the thermally induced transition, certainly due to the excess heat provided by the laser beam. On the contrary, at lower bath temperatures, large variations are observed in transition times [as shown, for example, in Fig. 4(a)].

Below a certain bath temperature (hereafter denoted $T_{b,c}$), it is possible to transform only a small fraction of the crystal under the continuous laser beam, and therefore to leave the

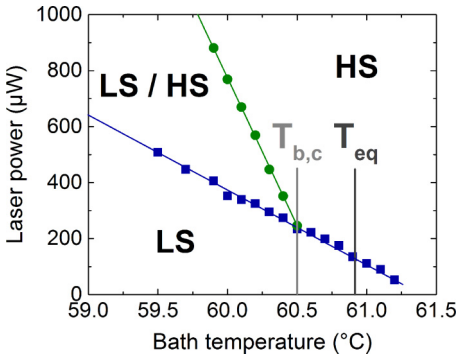

FIG. 5. Laser power–bath temperature diagram of crystal B (initially in the LS state) under continuous laser beam irradiation at point $B0$. The blue squares indicate the threshold laser power above which the nucleation of the HS phase is evidenced. Above a critical bath temperature $T_{b,c}$, the LS $\rightarrow$ HS transformation of the crystal is always complete. Below $T_{b,c}$, the crystal goes through a stationary biphasic state where the LS and HS phases coexist. The laser power has to be increased to a second threshold value (green circles) to reach the full HS state.

crystal in a steady laser-induced biphasic state. This effect is shown in Fig. 4(b) by a series of measurements performed at $T_b = 60.3\,^{\circ}$C (out of the thermal hysteresis loop). At $P = 295\,\mu$W, below the threshold power, the crystal remains completely in the LS state. Under continuous laser beam irradiation with $P = 382\,\mu$W (see the snapshots in Fig. 3 of the supplemental material) and $P = 520\,\mu$W, a stationary regime is reached in which 40% and 60% of the crystal is transformed into the HS state, respectively. Finally, at higher power ($P = 675\,\mu$W), the crystal is completely transformed. This critical bath temperature $T_{b,c}$ has been experimentally determined by a series of thorough temperature- and laser-power-dependent measurements. These experiments allowed the laser power–bath temperature ($P-T_b$) parameter diagram depicted in Fig. 5 to be evaluated. Blue squares indicate the threshold power to induce the nucleation of the HS phase by the laser beam. For $T_b > T_{b,c}$, the transformation of the crystal into the HS state is always complete when this threshold power is surpassed. Below $T_{b,c} = 60.5\,^{\circ}$C, we observe a regime where the LS and HS phases coexist within the crystal. A second threshold power then has to be reached in order to obtain the complete transformation of the crystal into the HS state (green circles). As displayed in Fig. 5, these two "threshold" powers grow linearly as the bath temperature decreases, but with different rates.

As detailed in Sec. III B 3 using a simple model, we show that these different rates are a consequence of temperature gradients experienced by the crystal under the effect of spatially localized laser irradiation. The lower the bath temperature, the higher the laser power required for the nucleation of the HS phase, and the higher the temperature gradient within the crystal. Therefore, the power required to induce the complete transformation of the crystal increases with a higher rate.

2. *In the dynamic regime*

We have also investigated the dynamic aspects of this photothermal process. The experimental procedure was as follows: starting from the crystal in the LS state at $T_b = 60.2\,^{\circ}$C, the laser beam was turned on (at point $B0$ with a power $P_m = 490\,\mu$W) to induce the crystal in a stationary biphasic state. Subsequently, we modulated the laser light intensity at a controlled frequency using a chopper, and we followed the time evolution of the optical transmission ($\lambda = 543 \pm 22$ nm) of the crystal by taking optical microscopy images with a high frame rate (fps = 84 Hz). Figure 6(a) shows the typical results obtained by modulating the laser intensity at a frequency of $\nu = 5.4$ Hz (red solid line). We observe the occurrence of clear periodic oscillations of the HS fraction (with a given amplitude denoted Δn_{HS}) at the excitation frequency and with a delay $\delta \approx 40$ ms.

We have carried out this type of measurement at various modulation frequencies. As displayed in Fig. 6(b), an increase of the modulation frequency entails a decrease of the amplitude of the HS fraction modulation Δn_{HS} in the crystal. This can be explained by the fact that rapid variations of the laser intensity no longer allow efficient heating or cooling of the crystal and subsequent generation of significant changes in temperature. The crystal is then no longer able to respond to the light excitation. An exponential fit [red solid line in Fig. 6(b)] gives a cutoff frequency of $\nu_c = 10.8$ Hz. In other words, $\tau_c = 1/\nu_c = 93$ ms can be understood as the characteristic response time of the crystal to the photothermal excitation.

This cutoff frequency is significantly higher than that determined by Sy *et al.* (1.5 Hz) in the SCO compound [{Fe(NCSe)(py)$_2$}$_2$(m-bpypz)] [9]. Unlike us, however, their study was carried out in vacuum, implying that thermal exchange with the environment is certainly less efficient. The shorter response time of the present compound might also be related to a greater thermal conductivity of the material, which could speed up the return to equilibrium when a thermal excitation is applied. As a final remark, we can see that the ratio R/ν_c (R being the temperature scan rate) giving the change of bath temperature during the transient regime is very small even for large scan rates ($R/\nu_c = 7.7$ mK at $R = 5$ K/min). In other words, it shows that the crystal is able to follow the bath temperature without delay over the range of the experimentally studied scan rates, in accordance with the results of the thermoinduced measurements performed in Sec. III A.

3. *Theoretical model*

For a detailed understanding of the photothermal process, we developed a model in which we accounted for all the relevant thermal contributions. In this simple model, the SCO crystal is considered to be an infinite two-dimensional system (infinite disk of thickness L) immersed in a thermal bath of temperature T_b and irradiated by a laser beam in the form of an ideal point (see Sec. 3 of the supplemental material for details [31]). The crystal temperature at point r and time t is governed by the heat balance established in Eq. (1), whose right-hand side expresses, respectively, the diffusion of heat in the crystal, the heat transfer from the crystal to the thermal bath (with a rate α), and the source term accounting for the heat flow deposited by the point laser beam at $r = 0$:

$$\frac{\partial T}{\partial t} = D_T \nabla^2 T - \alpha(T - T_b) + \frac{W_0}{(\rho/M)C_p}\delta(r). \qquad (1)$$

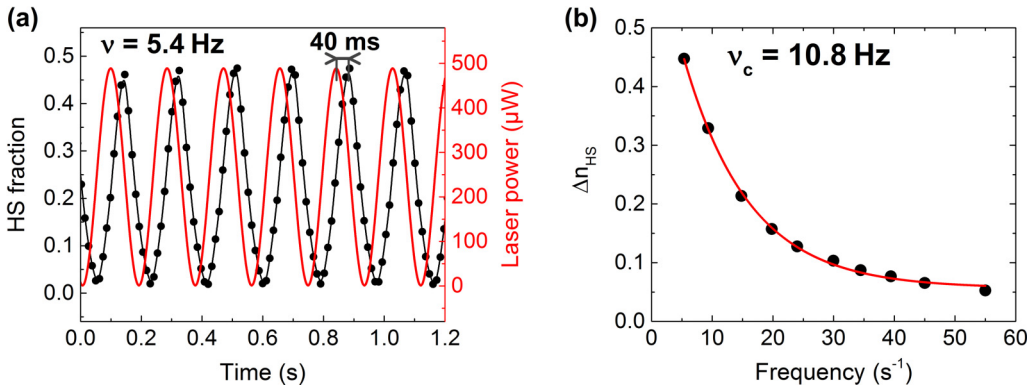

FIG. 6. Dynamic aspects of the photothermal transition generated by the localized laser beam. (a) Time dependence of the HS fraction (deduced from the spatially averaged optical transmission of the crystal) under the effect of a modulated ($P_m = 490\,\mu$W) laser beam irradiation at a frequency $\nu = 5.4$ Hz (red solid line). (b) Evolution of the amplitude of the HS fraction modulation $\Delta n_{\rm HS}$ as a function of the laser frequency. The red line is the result of an exponential fit.

$\delta(r)$ is the Dirac delta distribution. The heat provided by the microscope light and the latent heat associated with the first-order transition are neglected. In Eq. (1), ρ is the density, M is the molar mass, C_p is the molar heat capacity, and W_0 is the amount of energy imparted by the laser per unit time and volume. D_T is the thermal diffusion constant of the SCO material, and α is the thermal coupling constant of the crystal to the thermal bath. In other words, $1/\alpha$ is the characteristic response time of the sample to reach the thermal equilibrium with its environment in response to an instantaneous change in temperature. From our previous dynamic measurements (Sec. III B 2), we assigned the following: $\alpha = \nu_c = 10.8\,\mathrm{s}^{-1}$. In the stationary regime $\partial T/\partial t = 0$ and imposing a relevant boundary condition on the total heat flux brought by the point laser beam (see the Supplemental Material [31]), the crystal temperature at a distance r from the laser spot is given by the following analytical expression:

$$T(r) = T_b + \frac{P\alpha_{\rm abs}}{L(\rho/M)C_p D_T}\sqrt{\frac{\lambda}{8\pi r}}\exp\left(-\frac{r}{\lambda}\right), \qquad (2)$$

where L is the crystal thickness, P is the incoming laser power, α_{abs} is the mean optical absorption of the crystal at the laser wavelength, and $\lambda = \sqrt{D_T/\alpha}$.

From Eq. (2), we can successfully explain and reproduce the laser power–bath temperature ($P-T_b$) parameter diagram of Fig. 5 by choosing relevant conditions for the nucleation and the growth of the newly formed HS phase in the crystal. We stipulate that the laser-induced nucleation is obtained when the temperature at point $B1$, situated at $r_1 = 30\,\mu$m from the laser spot, is larger than $T_{1/2}{}^{\uparrow} = 61.26\,^{\circ}$C. The second criterion is that the laser-induced HS phase propagates everywhere the crystal temperature is larger than the Maxwell temperature $T_{\rm eq} = 60.91\,^{\circ}$C. The latter was determined from a fit of the thermal hysteresis loop (shown in Fig. 2(a) of the supplemental material) using the Slichter-Drickamer mean-field model [40]. This condition is rationalized by the fact that the propagation of the LS/HS phase boundary can be achieved only if the HS state is the thermodynamically stable state. Following this idea, the complete transformation of the crystal is obtained when $T(r = r_2 = 90\,\mu\mathrm{m}) > T_{\rm eq}$. The two criteria can be expressed as follows:

(a) Nucleation of the HS state:

$$T(r = r_1 = 30\,\mu\mathrm{m}) \geqslant T_{1/2}^{\uparrow} = 61.26\,^{\circ}\mathrm{C} \qquad (3)$$

(b) Growth of the HS phase:

$$T(r) \geqslant T_{\rm eq} = 60.91^{\circ}\mathrm{C}. \qquad (4)$$

It is worth mentioning that the present model gives infinite temperatures at the position of the laser spot ($r = 0$), but our approach is justified since we focus only on temperature values at distances ($>r_1$) sufficiently large from the point source compared to the size of the laser spot ($\varnothing = 2\,\mu$m). By choosing parameter values derived from various independent measurements [$\alpha_{abs} = 0.09$ and $L = 24\,\mu$m (optical microscopy), $\rho = 1.53\,\mathrm{g\,cm}^{-3}$ and $M = 487.88\,\mathrm{g\,mol}^{-1}$ (x-ray diffraction), $C_p = 540\,\mathrm{J\,mol}^{-1}\,\mathrm{K}^{-1}$ (differential scanning calorimetry), and $\alpha = 10.8\,\mathrm{s}^{-1}$ (optical microscopy dynamic measurements)], and considering the criteria of Eqs. (3) and (4), the best description of the laser power–bath temperature diagram [shown in Fig. 7(a)] is obtained by taking $D_T = 2.6 \times 10^{-7}\,\mathrm{m}^2\,\mathrm{s}^{-1}$. This value is realistic and falls in the expected range for this kind of system if we consider previous estimations from the literature [41,42]. Let us note that Sy *et al.* [9] used a D_T value of $2 \times 10^{-10}\,\mathrm{m}^2\,\mathrm{s}^{-1}$ in the framework of theoretical models, which seems to us to be greatly underestimated. The linear behavior of the threshold powers with the bath temperature as well as the coexistence of LS and HS domains are both well explained in the framework of this simple model. The "critical" point is found at ($T_{b,c} = 60.66\,^{\circ}$C, $P_c = 190\,\mu$W). It should be stressed that this model could be extended by considering the effect of the spin transition to obtain a more detailed analysis of the processes involved, but this task is beyond the scope of the present study.

Figures 7(b) and 7(c) show the temperature gradients, calculated from Eq. (2), experienced by the crystal at different laser powers for two characteristic zones of the diagram: $T_b = 60.75\,^{\circ}\mathrm{C} > T_{b,c}$ [Fig. 7(b)] and $T_b = 60.0\,^{\circ}\mathrm{C} < T_{b,c}$ [Fig. 7(c)]. When $T_b > T_{b,c}$, the nucleation process is irremediably followed by the complete transformation of the crystal. As shown in Fig. 7(b), this is because the power required to trigger the nucleation of the HS phase at point $B1$ ($r_1 = 30\,\mu$m) is sufficient to heat up the sample above the Maxwell temperature

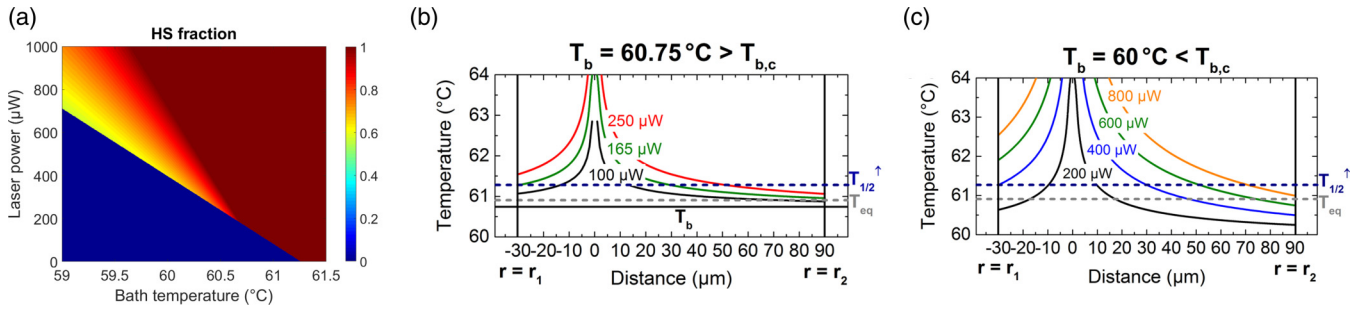

FIG. 7. Results of the thermal model. (a) Laser power–bath temperature parameter diagram computed from Eq. (2) and criteria of Eqs. (3) and (4). The best agreement with the experimental diagram of Fig. 5 is obtained by taking $D_T = 2.6 \times 10^{-7}\ \mathrm{m^2 s^{-1}}$. (b) and (c) Temperature gradients, calculated from Eq. (2), experienced by the crystal at $T_b = 60.75\ ^\circ\mathrm{C}$ ($> T_{b,c}$) and $T_b = 60\ ^\circ\mathrm{C}$ ($< T_{b,c}$), respectively, at different laser power values.

T_{eq}, such that the HS state is the thermodynamically stable state in the whole crystal. Below $T_{b,c}$, higher powers are required to induce the nucleation of the HS phase, generating larger temperature gradients within the crystal. As illustrated in Fig. 7(c) at $T_b = 60\ ^\circ\mathrm{C}$, at the nucleation laser power (400 μW), the sample temperature remains below T_{eq} at the other end of the sample ($r = r_2$) and the newly formed HS phase cannot propagate throughout the crystal. Therefore, there is a power range for which the stationary coexistence of the LS and HS phase is observed under continuous laser irradiation. The laser power has to be increased to heat the entire crystal above T_{eq} and to induce the complete transformation of the sample.

IV. CONCLUSION

In summary, we have reported a thorough optical microscopy study of the spatiotemporal dynamics of the first-order spin transition in two single crystals of the SCO compound $[Fe(HB(tz)_3)_2]$. The investigation of the thermally induced transition reveals unique switching properties: high stability of the thermal hysteresis loop, unprecedented large velocities of the macroscopic LS/HS interfaces up to 500 μm/s, and no visible temperature scan rate dependency of the transition dynamics in the range 0.1–5 °C/min. These measurements demonstrate that the switching kinetics can be intrinsically fast in SCO solids. These properties have to be correlated with the strong resilience of these crystals upon repeated thermal switching. The use of a localized laser beam to induce the transition through a local photothermal excitation enabled remarkable phenomena to be displayed, such as threshold effects, particularly long incubation periods, thermal activation of the LS/HS interface propagation, and stabilization of the crystal into a stationary biphasic state under light irradiation. Dynamic measurements of this photothermal process revealed the relatively fast response time of the material to thermal excitations, confirming that the crystal remains in thermal equilibrium with its environment over the range of experimentally studied scan rates, which assures the kinetic independence of the thermal hysteresis loop. These laser-induced measurements demonstrated the importance of thermal effects in the transition dynamics, and they enabled an accurate determination of the thermal properties of the SCO compound in the framework of a simple theoretical model. Nevertheless, it appears difficult to explain the particular spatiotemporal characteristics of the spin transition in this compound. Femtosecond pump-probe studies are currently underway on crystals and thin films of this SCO compound to determine the intrinsic speed of LS-HS switching. The present study raises the problem of the lack of complete experimental characterizations (mechanical, thermal, structural, etc.), and especially the lack of theoretical models that would incorporate these different parameters to explain the key features of the spatiotemporal dynamics of the spin transition. The development of such predictive models appears to be essential to clearly understand the relative importance of these different parameters in the dynamics of nucleation and growth processes in SCO solids.

ACKNOWLEDGMENTS

The authors are thankful to Laure Vendier for preliminary x-ray diffraction experiments. This work was supported by the Région Occitanie (Contract No. 15050450). S.R. thanks the French Ministry of Research for a Ph.D. grant.

[1] P. Gütlich and H. A. Goodwin, *Spin Crossover in Transition Metal Compounds I-III* (Springer, Berlin, 2004).
[2] M. A. Halcrow, *Spin-Crossover Materials: Properties and Applications* (Wiley, Leeds, 2013).
[3] O. Kahn and C. J. Martinez, Science **279**, 44 (1998).
[4] N. Huby, L. Guérin, E. Collet, L. Toupet, J.-C. Ameline, H. Cailleau, T. Roisnel, T. Tayagaki, and K. Tanaka, Phys. Rev. B **69**, 020101(R) (2004).
[5] S. Pillet, J. Hubsch, and C. Lecomte, Eur. Phys. J. B **38**, 541 (2004).
[6] S. Bedoui, G. Molnár, S. Bonnet, C. Quintero, H. J. Shepherd, W. Nicolazzi, L. Salmon, and A. Bousseksou, Chem. Phys. Lett. **499**, 94 (2010).
[7] A. Slimani, F. Varret, K. Boukheddaden, C. Chong, H. Mishra, J. Haasnoot, and S. Pillet, Phys. Rev. B **84**, 094442 (2011).

[8] A. Slimani, F. Varret, K. Boukheddaden, D. Garrot, H. Oubouchou, and S. Kaizaki, Phys. Rev. Lett. **110**, 087208 (2013).

[9] M. Sy, D. Garrot, A. Slimani, M. Páez-Espejo, F. Varret, and K. Boukheddaden, Angew. Chem. Int. Ed. **55**, 1755 (2016).

[10] K. Boukheddaden, M. Sy, M. Paez-Espejo, A. Slimani, and F. Varret, Phys. B Condens. Matter **486**, 187 (2016).

[11] S. Bonhommeau, G. Molnár, A. Galet, A. Zwick, J.-A. Real, J. J. McGarvey, and A. Bousseksou, Angew. Chem. Int. Ed. **44**, 4069 (2005).

[12] S. Cobo, D. Ostrovskii, S. Bonhommeau, L. Vendier, G. Molnár, L. Salmon, K. Tanaka, and A. Bousseksou, J. Am. Chem. Soc. **130**, 9019 (2008).

[13] N. Ould Moussa, D. Ostrovskii, V. M. Garcia, G. Molnár, K. Tanaka, A. B. Gaspar, J. A. Real, and A. Bousseksou, Chem. Phys. Lett. **477**, 156 (2009).

[14] S. Bedoui, M. Lopes, W. Nicolazzi, S. Bonnet, S. Zheng, G. Molnár, and A. Bousseksou, Phys. Rev. Lett. **109**, 135702 (2012).

[15] Y. Ogawa, S. Koshihara, K. Koshino, T. Ogawa, C. Urano, and H. Takagi, Phys. Rev. Lett. **84**, 3181 (2000).

[16] A. Goujon, F. Varret, K. Boukheddaden, C. Chong, J. Jeftić, Y. Garcia, A. D. Naik, J. C. Ameline, and E. Collet, Inorg. Chim. Acta **361**, 4055 (2008).

[17] S. Bonnet, G. Molnár, J. Sanchez Costa, M. A. Siegler, A. L. Spek, A. Bousseksou, W.-T. Fu, P. Gamez, and J. Reedijk, Chem. Mater. **21**, 1123 (2009).

[18] C. Chong, H. Mishra, K. Boukheddaden, S. Denise, G. Bouchez, E. Collet, J.-C. Ameline, A. D. Naik, Y. Garcia, and F. Varret, J. Phys. Chem. B **114**, 1975 (2010).

[19] C. Chong, A. Slimani, F. Varret, K. Boukheddaden, E. Collet, J.-C. Ameline, R. Bronisz, and A. Hauser, Chem. Phys. Lett. **504**, 29 (2011).

[20] F. Varret, A. Slimani, K. Boukheddaden, C. Chong, H. Mishra, E. Collet, J. Haasnoot, and S. Pillet, New J. Chem. **35**, 2333 (2011).

[21] S. Bedoui, M. Lopes, S. Zheng, S. Bonnet, G. Molnár, and A. Bousseksou, Adv. Mater. **24**, 2475 (2012).

[22] M. Sy, F. Varret, K. Boukheddaden, G. Bouchez, J. Marrot, S. Kawata, and S. Kaizaki, Angew. Chem. Int. Ed. **53**, 7539 (2014).

[23] S. Bedoui, W. Nicolazzi, S. Zheng, S. Bonnet, G. Molnár, and A. Bousseksou, Polyhedron **87**, 411 (2015).

[24] S. Rat, J. Sánchez Costa, S. Bedoui, W. Nicolazzi, G. Molnár, L. Salmon, and A. Bousseksou, Pure Appl. Chem. **87**, 261 (2015).

[25] K. Boukheddaden and M. Sy, Curr. Inorg. Chem. **6**, 40 (2016).

[26] E. M. Hernández, S. Zheng, H. J. Shepherd, D. S. Yufit, K. Ridier, S. Bedoui, W. Nicolazzi, V. Velázquez, S. Bonnet, G. Molnár, and A. Bousseksou, J. Phys. Chem. C **120**, 27608 (2016).

[27] R. Traiche, M. Sy, H. Oubouchou, G. Bouchez, F. Varret, and K. Boukheddaden, J. Phys. Chem. C **121**, 11700 (2017).

[28] G. Molnár, A. Bousseksou, A. Zwick, and J. J. McGarvey, Chem. Phys. Lett. **367**, 593 (2003).

[29] S. Rat, K. Ridier, L. Vendier, G. Molnár, L. Salmon, and A. Bousseksou, Cryst. Eng. Commun. **19**, 3271 (2017).

[30] C. A. Schneider, W. S. Rasband, and K. W. Eliceiri, Nat. Methods **9**, 671 (2012).

[31] See Supplemental Material at http://link.aps.org/supplemental/10.1103/PhysRevB.96.134106 for movies S1–S4, spatiotemporal investigations of the spin transition in crystal B (Sec. 1), comparative switching kinetics of single crystals of other SCO compounds in the same experimental conditions (Sec. 2), and a description of the theoretical model (Sec. 3).

[32] A. Yangui, M. Sy, L. Li, Y. Abid, P. Naumov, and K. Boukheddaden, Sci. Rep. **5**, 16634 (2015).

[33] J. Yoon, H. Kim, X. Chen, N. Tamura, B. S. Mun, C. Park, and H. Ju, ACS Appl. Mater. Interf. **8**, 2280 (2016).

[34] F. Varret, C. Chong, A. Slimani, D. Garrot, Y. Garcia, and A. D. Naik, *Spin-Crossover Materials: Properties and Applications* (Wiley, Leeds, 2013), pp. 425–441.

[35] H. Spiering, K. Boukheddaden, J. Linares, and F. Varret, Phys. Rev. B **70**, 184106 (2004).

[36] G. Félix, M. Mikolasek, H. Peng, W. Nicolazzi, G. Molnár, A. I. Chumakov, L. Salmon, and A. Bousseksou, Phys. Rev. B **91**, 024422 (2015).

[37] J.-P. Tuchagues, A. Bousseksou, G. Molnár, J. J. McGarvey, and F. Varret, *Spin Crossover in Transition Metal Compounds III* (Springer, Berlin, 2004), pp. 84–103.

[38] V. Shalabaeva, S. Rat, M. D. Manrique-Juarez, A.-C. Bas, L. Vendier, L. Salmon, G. Molnár, and A. Bousseksou, J. Mater. Chem. C **5**, 4419 (2017).

[39] A. Slimani, K. Boukheddaden, and K. Yamashita, Phys. Rev. B **92**, 014111 (2015).

[40] C. P. Slichter and H. G. Drickamer, J. Chem. Phys. **56**, 2142 (1972).

[41] O. Fouché, J. Degert, G. Jonusauskas, N. Daro, J.-F. Létard, and E. Freysz, Phys. Chem. Chem. Phys. **12**, 3044 (2010).

[42] O. Kraieva, Ph.D. thesis, University of Toulouse (2015), http://www.theses.fr/2015TOU30315.